Montmorillonite−Poly(ethylene oxide) Nanocomposites: Interlayer Alkali Metal Behavior

Marc X. Reinholdt,*,†,‡ R. James Kirkpatrick,† and Thomas J. Pinnavaia‡

Department of Geology, University of Illinois at Urbana-Champaign, 1301 West Green Street, Urbana, Illinois 61801, and Department of Chemistry, Michigan State University, East Lansing, Michigan 48824

Received: May 17, 2005; In Final Form: July 5, 2005

Clay−PEO nanocomposites can have large electrical conductivities that make them potential electrolyte materials for rechargeable lithium batteries, but the origin of these large conductivities, especially for Li-containing materials, is poorly understood. This paper presents X-ray diffraction (XRD), TGA-DTA, and ^{7}Li and ^{23}Na NMR data for PEO nanocomposites made with natural (SWy-1) and synthetic (MNTS) montmorillonite clays that provide new insight into interlayer structure. An increase in basal d_{001}-spacings demonstrates successful intercalation of PEO in all samples, and X-ray line narrowing shows that this intercalation improves the layer stacking order. The basal spacings of 17.9−19.4 Å are consistent with a helical or bilayer structure of PEO in the interlayer. TGA-DTA provides quantitative results for the hydration state of the nanocomposites, demonstrates PEO intercalation, and shows that the composites prepared from the synthetic montmorillonite are less stable than those made with SWy-1. ^{7}Li NMR shows that the nearest neighbor hydration state of Li^{+} is unaffected by PEO intercalation and suggests weak interaction of Li^{+} with PEO. ^{23}Na NMR shows that PEO intercalation results in the conversion of the multiple Na^{+} hydration states observed for the pristine clay into inner sphere sites most likely formed through coordination with the basal oxygens of the clay. These differences between lithium and sodium suggested that tighter binding of the Na to the clay may be the origin of the conductivity of Li−montmorillonite−PEO nanocomposites being as much as 2 orders of magnitude larger than those of Na−montmorillonite−PEO nanocomposites. The results confirm the idea that polymer oxygen atoms do not participate in sequestering the exchangeable cations and agree with the jump process for cation migration advanced by Kuppa and Manias (Kuppa, V.; Manias, E. *Chem. Mater.* **2002**, *14*, 2171).

Introduction

Improving rechargeable lithium batteries for applications in electronic, communication, and computing equipment is an ongoing goal for the 21st century, and improvement of the electrolyte materials for these batteries is key to this effort.[1,2] Several types of electrolyte materials are used in lithium batteries, including liquids, the most studied; solids formed primarily from mixtures of polymers and alkaline salts; gels, semiliquid mixtures of polymer and alkaline salts; and solid nanocomposites. Recent studies of polymer nanocomposites have focused on dispersions of high surface area inorganic particles, such as zirconia, anatase, alumina, or silica, in a polymer/alkaline salt matrix, but lamellar and porous compounds, such as clays,[3,4] zeolites,[5] layered double hydroxides (LDH),[6,7] and mesostructured materials,[8] have also been investigated. For lamellar and porous electrolytes, polymer organization in the confined spaces may play a role in enhancing ionic conductivity. This latter possibility has been investigated mainly for clay minerals,[9−18] although there has been some work on polymer intercalation in layered double hydroxides.[19] The main advantage of layered nanocomposites with inorganic matrixes is that their conductivity decreases linearly with the temperature, even below the melting point of the polymer. This behavior is in contrast to nanocomposites with polymer matrixes for which the temperature dependence of the conductivity undergoes a significant change in the slope below the melting point of the polymer.

The present work investigates the interlayer structure and thermal behavior of PEO−montmorillonite polymer nanocomposites prepared from Li-, Na-, and K-exchanged natural and synthetic forms of this smectite mineral,[20,21] with the objective of better understanding the origin of the differences in conductivity of these materials. The samples are characterized at the macroscopic scale by X-ray diffraction (XRD) and thermal analysis (TGA and DTA) and at the atomic level by solid-state nuclear magnetic resonance (NMR) spectroscopy.

Materials and Methods

The two montmorillonites used in this study are natural Swy-1 (Clay Source Repository of the Clay Mineral Society) and a synthetic one, denoted MNTS here. Swy-1 has a layer charge of 0.70 electron charge units per unit cell structural formula of $Na_{0.70}[Mg_{0.45}Fe_{0.42}Al_{3.08}][Al_{0.26}Si_{7.74}]O_{20}(OH)_4$.[22] MNTS was crystallized from a hydrogel composed of deionized water, hydrofluoric acid, sodium acetate, magnesium acetate tetrahydrate, pseudo-boehmite (Pural SB-1, Sasol), and amorphous silica using a method described elsewhere.[20,21] The composition of the hydrogel reaction mixture was 1.0 SiO_2, 0.2 Al_2O_3, 0.1 MgO, 0.05 Na_2O, 0.05 HF, 96 H_2O by weight, which corresponds to a product composition of $Na_{0.8}[Mg_{0.8}Al_{3.2}][Si_8]O_{20}(OH,F)_4$, assuming that all of the reagents are incorporated into the final product. Li- or K-exchanged forms of the two clays were made by cation exchange in 1 M aqueous LiCl or KCl

* Author to whom correspondence should be addressed. Phone: 217-244-2355; fax: 217-244-4996; e-mail: mreinhol@uiuc.edu.
† Department of Geology, University of Illinois at Urbana-Champaign.
‡ Department of Chemistry, Michigan State University.

10.1021/jp052601o CCC: $30.25
Published on Web 08/09/2005

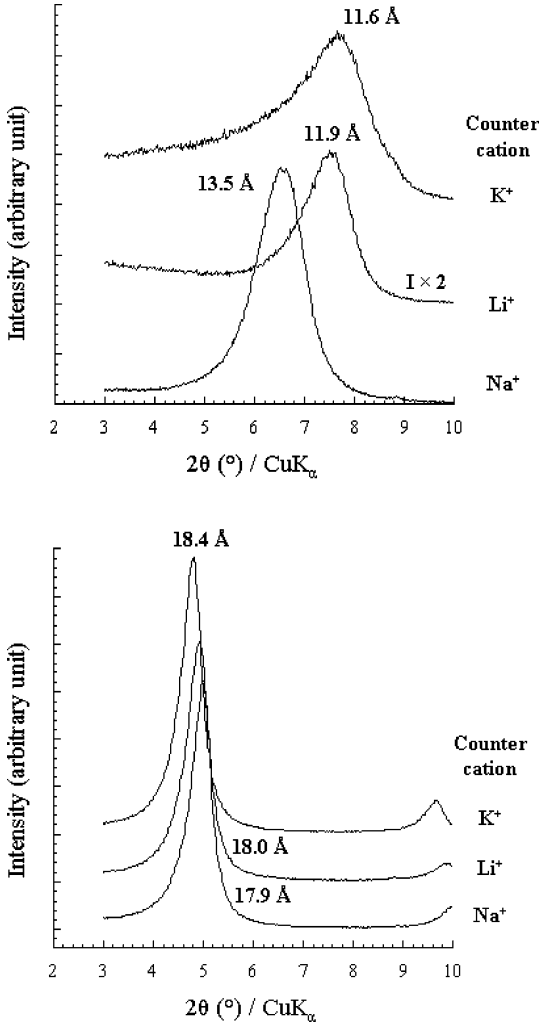

Figure 1. d_{001} X-ray diffraction peaks for cation-exchanged forms of naturally occurring SWy-1 montmorillonite (top) and for the corresponding 50:50 (w/w) clay:PEO nanocomposites (bottom).

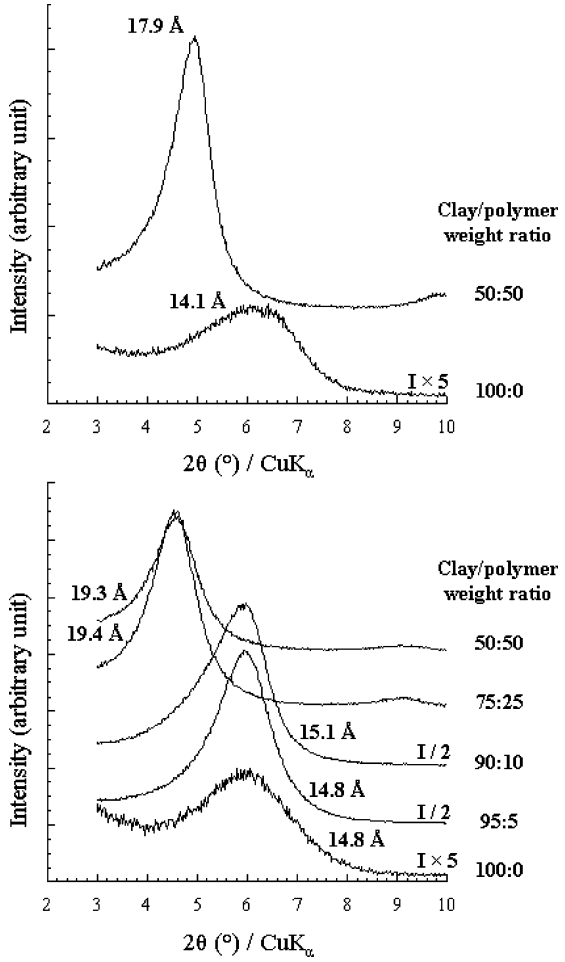

Figure 2. d_{001} X-ray diffraction peaks for synthetic Na−MNTS (top) and Li−MNTS (bottom) montmorillonites at different clay:PEO (w/w) ratios.

solutions and by using enough solution to provide a 10-fold excess of cation needed for complete exchange. The exchange suspensions were stirred for 2 h at room temperature and then were centrifuged, and the process was repeated twice for each sample. The samples were then washed with distilled water (suspended in water and centrifuged) until the product was chloride-free as tested using 10^{-1} M $AgNO_3$ solution. The poly(ethylene oxide) (PEO) (MW = 10^5 g mol^{-1}) was purchased from Aldrich and was used as received.

The process used to prepare the PEO−clay nanocomposites is based on the aqueous solution method of Bujdák and coworkers.[15] Composites containing a 50:50 (w/w) ratio of PEO and Li−, Na−, or K−SWy-1 montmorillonite were formed by adding a solution of 250 mg of polymer in 100 mL of deionized water (0.25% w/w) to a suspension of 250 mg of clay in 250 mL of water (0.10% w/w). The mixtures were aged under stirring for 48 h and then were centrifuged and washed five times with deionized water. Li−MNTS−PEO composites were prepared using similar methods at clay/polymer (w/w) ratios 100:0, 95:5, 90:10, 75:25, and 50:50 but were only centrifuged and were not washed to maintain the clay/polymer ratio of the restacked composite. For the Na−MNTS−PEO composite, only the 50:50 (w:w) sample was made using the same methods. After preparation, all nanocomposite samples were held at a relative humidity (RH) of 79% above a saturated NH_4Cl solution.

The XRD patterns were recorded using a Rigaku rotaflex diffractometer operated at 45 kV and 100 mA scanned using a step size of 0.02°/point, a scan rate of 0.5° min^{-1}, and employing Ni-filtered Cu Kα radiation (1.5406 Å). Samples were analyzed as oriented films made by placing a few drops of a suspension on a glass slide or as dry powders.

Thermogravimetric analysis (TGA) and differential thermal analysis (DTA) measurements were carried out using a NETZSCH Simultaneous Thermal Analyzer STA 409 using about 50 mg of sample. All samples were heated to 800 °C at a rate of 5 °C min^{-1} under air flow. Thermal analysis allows determination of the amount of water and polymer present in the composite.

^{7}Li and ^{23}Na MAS NMR were obtained using a Varian Unity Inova 500WB spectrometer (H_0 = 11.75 T) using 7-mm Doty MAS probe for ^{7}Li and a 7-mm CP-MAS Chemagnetics probe for ^{23}Na. The corresponding working frequencies were 194.263 and 132.219 MHz. For ^{7}Li, the pulse length was 3 μs ($\pi/2$ pulse length in solution was 5.5 μs), the recycle delay was 60 s, the spinning speed was about 7 kHz, and the number of transients recorded was 16. For ^{23}Na, the pulse length was 1.5 μs ($\pi/2$ pulse length in solution was 3.5 μs), the recycle delay was 0.5 s, the spinning speed was about 10 kHz, and the number of transients recorded was 10 240. Chemical shifts were reported in ppm relative to 1.0 M LiCl and NaCl solutions. The acquired free induction decay (FID) signals were processed using the NMR Utility Transform Software (NUTS, Acorn NMR soft-

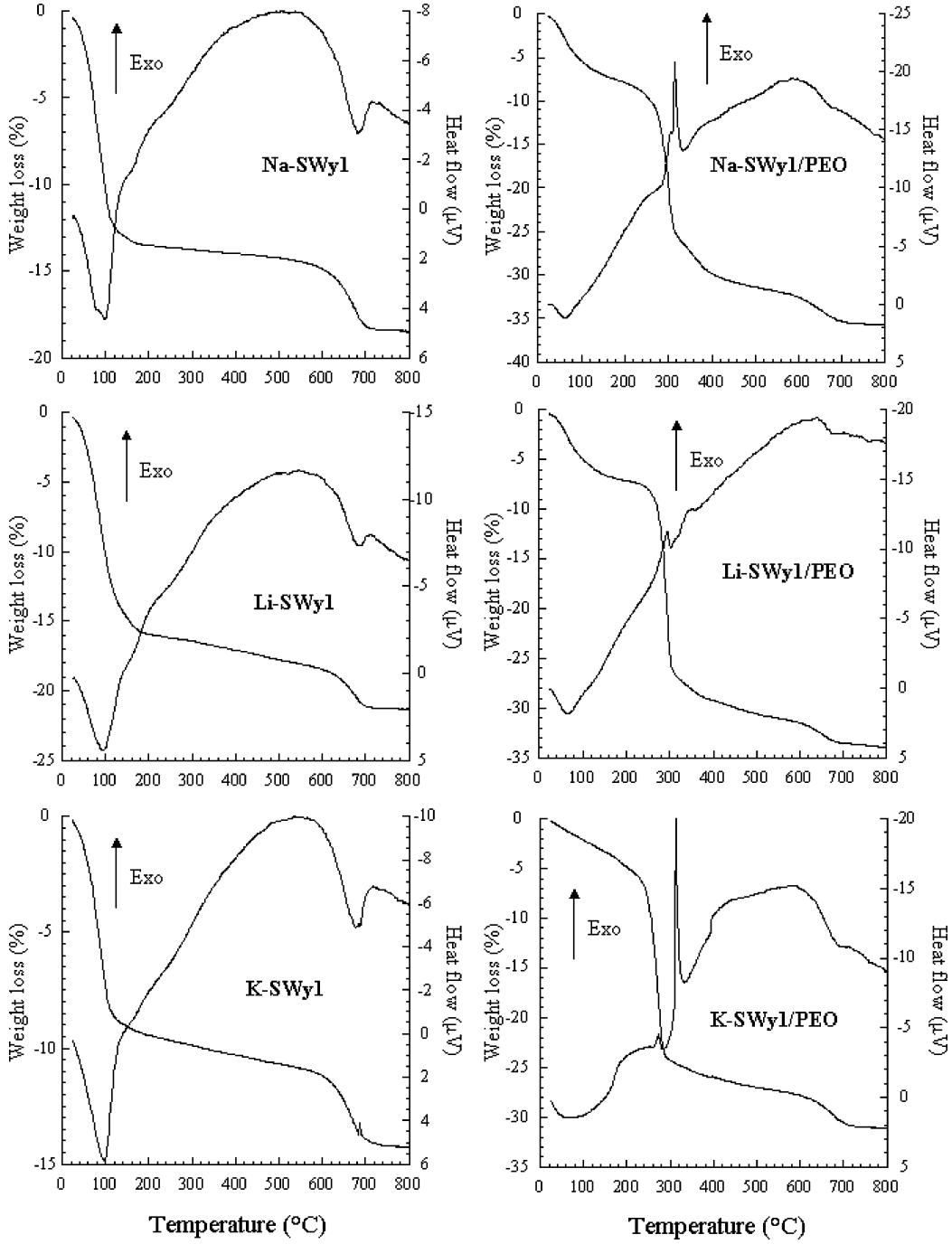

Figure 3. TGA-DTA curves for Li^+−, Na^+−, and K^+−SWy-1 montmorillonite in pristine and PEO nanocomposite form at a 50:50 (w/w) clay:PEO ratio.

ware). The baseline was corrected if needed, and the spectra are simulated with the NUTS software.

Results

X-ray Diffraction. Under ambient conditions of relative humidity, the basal spacings of Li^+-, Na^+-, and K^+-exchanged forms of SWy-1 are 11.9, 13.5, and 11.6 Å, respectively (Figure 1, top). For the corresponding 50:50 Swy-1−PEO composites, the spacings increase to 18.0, 17.9, and 18.4 Å, respectively (Figure 1, bottom). The basal spacings of pristine Li^+− and Na^+−MNTS are 14.8 Å and 14.1 Å, respectively. The basal spacing of the 50:50 Na−MNTS−PEO sample is 17.9 Å (Figure 2, top), and for the Li−MNTS−PEO samples, the basal spacings increase in a stepwise manner from about 15 Å for those intercalated at 10% PEO or less to about 19.3 Å for those intercalated at 25% PEO or more (Figure 2, bottom). These changes clearly demonstrate that PEO enters the interlayers of all the samples and that for Li−MNTS it does so in a stepwise manner.

Thermal Analysis. The thermal analysis (TGA-DTA) of the pristine clays and the clay/polymer nanocomposites differs substantially with regard to water content, the extent of PEO incorporation, and the effect of PEO on the water content (Figures 3 and 4; Table 1). The pristine clays all exhibit resolvable weight loss and endothermic features centered near 80−90, 150, and 640−660 °C. The pristine Li−MNTS sample also exhibits small weight loss and endothermic features centered near 460 °C. The 80−90 °C and 150 °C weight losses

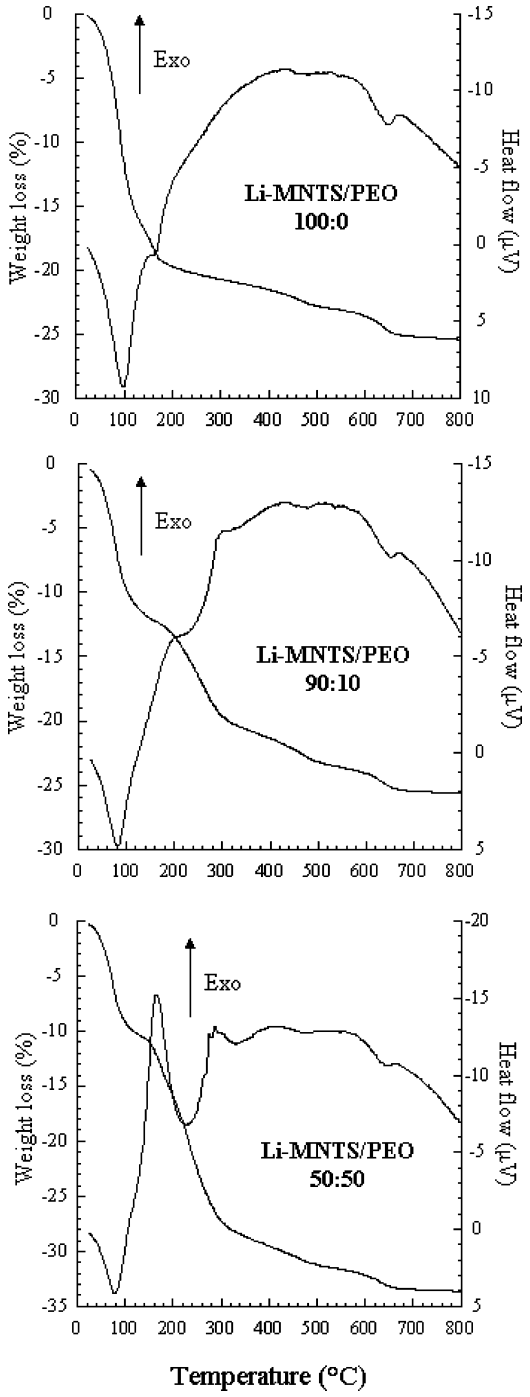

Figure 4. TGA-DTA curves for pristine and PEO nanocomposite forms of Li−MNTS montmorillonite.

and associated endothermic peaks are readily assigned to the loss of interlayer water (dehydration), and the 630−660 °C weight losses and associated endothermic peaks are assigned to the loss of structural hydroxyl groups (dehydroxylation). The features between 400 and 500 °C for Li−MNTS may be due to loss of hydroxyl groups in structural positions in which particular types of octahedral cations or octahedral vacancies are segregated.[20,23] The segregation of Mg, Zn, and vacancies was demonstrated by using ^{19}F MAS NMR and extended X-ray absorption fine structure (EXAFS) at the Zn and Mg K-edges for the synthetic montmorillonite.[20] The segregation of octahedral sites was also observed with infrared spectroscopy in the case of the natural SWa-1 ferruginous-smectite.[23] For SWy-1, the magnitude of the low-temperature weight loss increases from K^+ to Na^+ to Li^+, which have hydration states of 4.5, 7.0, and 8.3 water molecules per formula unit, respectively.

Most of the Swy-1−PEO and MNTS−PEO composites exhibit the same water weight loss and exothermic features as the pristine clays below 200 °C. The nanocomposites also exhibit additional weight loss features between 230 and 310 °C, and all but the 95:5 Li−MNTS−PEO sample yield resolvable exothermic DTA peaks in this temperature range. These weight losses and associated exothermic DTA features are readily attributed to the loss of polymer (PEO combustion). For the SWy-1 samples, PEO intercalation decreases the amount of hydration water from 7.0 to 5.3 molecules per formula unit for the Na^+-exchanged sample, from 8.3 to 3.9 molecules per formula unit for the Li^+-exchanged sample, and from 4.5 to 2.6 molecules per formula unit for the K^+-exchanged sample. The amount of intercalated PEO slightly decreases from Na^+- and Li^+-exchanged samples, with 5.9 and 5.8 ethoxy units, $-CH_2-CH_2-O-$, per formula unit, respectively, to K^+-exchanged samples, with 5.5 ethoxy units per formula unit. For the Li−MNTS nanocomposites, the amount of adsorbed water decreases and the amount of intercalated PEO increases as following the decrease of the Li−MNTS/PEO ratio. The 75:25 and 50:50 samples have approximately the same amounts of adsorbed water and intercalated PEO demonstrating interlayer saturation at these ratios.

Nuclear Magnetic Resonance. The ^{7}Li spectra of pristine Li−MNTS and all the Li−MNTS composites contain only a single symmetric peak near −0.41 to −0.54 ppm that becomes slightly broader and more shielded (more negative) with increasing polymer/clay ratio (Figure 5; Table 2). These results suggest that the local Li-structural environments are essentially the same in all these samples. Thus, for Li−MNTS, PEO intercalation results in a reduction in the interlayer water content but not in a change in the nearest neighbor hydration of Li^+, as previously suggested by Wong et al.[24] ^{7}Li is a quadrupolar nucleus (spin $I = 3/2$), and the symmetrical peak shapes suggest that the Li^+ has a spherically symmetric electric field gradient or its field gradient is undergoing dynamical reorientation.[25−27] The slight broadening of the peak with increasing polymer/clay ratio may indicate a slight decrease in the reorientational frequency, and the slightly more negative chemical shifts may indicate a slight increase in coordination.

The ^{23}Na NMR spectra of the Na−Swy-1 and Na−MNTS samples with and without PEO are shown in Figures 6 and 7 and the resonances are listed in Table 3. The Na−SWy-1 sample yields four resonances: a narrow one at −9.4 ppm (fwhm = 60 Hz), two broader ones centered at −10.3 and −18.5 ppm with fwhms of 600 and 2010 Hz, respectively, and a broad, low one centered at −33.2 ppm (fwhm = 1790 Hz). The Na−MNTS 100:0 sample yields three resonances centered at −11.4, −12.5, and −18.4 ppm with fwhms of 250, 610, and 1220 Hz, respectively. These different components can be readily assigned to Na^+ in various hydration states that interact differently with the silicate surface.[28−30] The narrow peaks at −9.4 ppm for SWy-1 and −11.4 ppm for MNTS represent Na^+ in dynamically averaged, solution-like environments. These may be small volumes of liquid pore water formed at the high RH of equilibration (79%). The quite negative chemical shift relative to bulk NaCl solution at 0 ppm clearly shows significant Na-interaction with the clay surface. The peaks at −10.3 for SWy-1 and −12.5 ppm for MNTS represent Na^+ on so-called outer-sphere sites,[28,30] in which the ion is fully hydrated, most likely by six nearest neighbor (NN) water molecules, and is separated from the silicate and polymer by these hydration waters.[30] The

TABLE 1: TGA-DTA Results. Thermogravimetric and Thermal Phenomena and Their Attribution

	endothermic peak			exothermic peak		
sample	*t* (°C)	weight loss (%)	attribution	*t* (°C)	weight loss (%)	attribution
Na−SWy-1	80	14.0	dehydration			
	660	4.5	dehydroxylation			
Na−SWy-1/PEO	80	7.5	dehydration	300	23.5	PEO combustion
	500	4.5	dehydroxylation			
Li−SWy-1	90	17.0	dehydration			
	670	4.0	dehydroxylation			
Li−SWy-1/PEO	80	7.0	dehydration	290	24.0	PEO combustion
	650	3.0	dehydroxylation			
K−SWy-1	90	10.5	dehydration			
	670	3.5	dehydroxylation			
K−SWy-1/PEO	100	3−4[a]	dehydration	270	23−24	PEO combustion
	660	4.0	dehydroxylation			
Li−MNTS 100:0	90	21.0	dehydration			
	460	2.5	dehydroxylation			
	630	2.0	dehydroxylation			
Li−MNTS 95:5	80	15.5	dehydration	260	4.5	PEO combustion
	460	2.5	dehydroxylation			
	630	2.0	dehydroxylation			
Li−MNTS 90:10	80	12.5	dehydration	260	9.0	PEO combustion
	470	2.0	dehydroxylation			
	630	2.5	dehydroxylation			
Li−MNTS 75:25	70	9.5	dehydration	230	17.0	PEO combustion
	470	2.5	dehydroxylation			
	640	1.5	dehydroxylation			
Li−MNTS 50:50	70	10.0	dehydration	220	19.0	PEO combustion
	465	2.0	dehydroxylation			
	630	2.5	dehydroxylation			

[a] Small endothermic peak associated with a slight mass loss in the TGA.

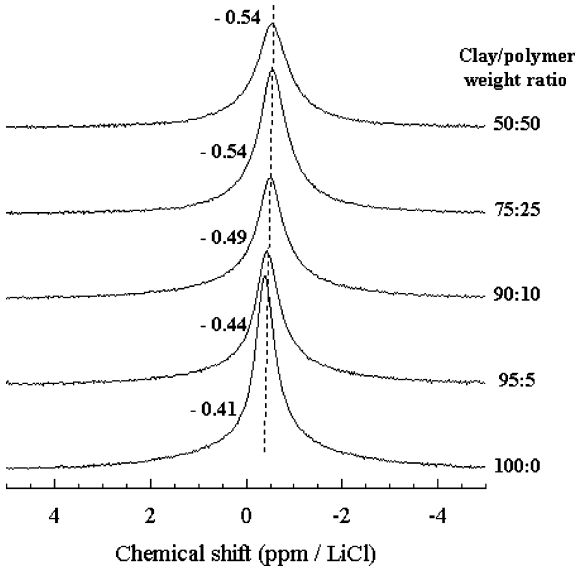

Figure 5. ^{7}Li MAS NMR spectra for Li−MNTS pristine clay and PEO nanocomposites at selected clay:PEO ratios.

TABLE 2: ^{7}Li Resonances for the Li−MNTS/PEO Samples as a Function of the Clay/Polymer Ratio

Li−MNTS/PEO ratio	chemical shift (ppm)	fwhm (Hz)
100:0	−0.41	120
95:5	−0.44	140
90:10	−0.49	145
75:25	−0.54	140
50:50	−0.54	160

narrowness of these resonances suggests a quite symmetrical environment or motional averaging of the chemical shift anisotropy (CSA) and quadrupolar interactions. The much broader peaks at −18.5 for Swy-1 and − 18.4 ppm for MNTS are assigned to Na^+ on so-called inner-sphere complexes, in which the Na^+ has lost some of its NN hydration waters and is directly coordinated by basal oxygen atoms of the tetrahedral sheet.[28] The resonance centered at − 33.2 ppm for SWy-1 probably corresponds to Na^+ that has lost all or most of its NN hydration waters and is interacting strongly with the oxygen atoms of the silicate layer. Such sites were first observed for fully dehydrated Na−hectorite.[10] The overall trend of increasing shielding of ^{23}Na resonances with increasing dehydration may also correspond to increasing Na^+ coordination.[29]

The ^{23}Na NMR spectra of the Na−SWy-1−PEO and Na−MNTS 50:50 samples contain only a single broad symmetric peak at −19.8 ppm and −18.8 ppm, respectively, that corresponds to the −18.5 and −18.4 ppm peaks for inner-sphere Na^+ in the pristine clays. Thus, it appears that for both Swy-1 and MNTS, PEO intercalation results in a reduction in interlayer water content, a net decrease in Na^+ hydration, and migration of the Na^+ to inner-sphere sites. Comparable changes in the ^{23}Na resonances occur for Na^+−hectorite−PEO composites,[10] in which the ^{23}Na chemical shifts become less shielded from −21.6 and −30.6 ppm for fully dehydrated pristine Na−hectorite to −10.8 ppm for the dry Na−hectorite−PEO composite.

Discussion

The intercalation of poly(ethylene oxide) (PEO) with montmorillonite and hectorite exchanged with various cations was first reported by Ruiz-Hitzky and co-workers.[9,10,11] These nanocomposites had conductivities of 10^{-9} to 10^{-4} S cm^{-1}. These authors postulated that the PEO chains retain their helical structure in the intercalated state, forming some kind of tunnel that increases the mobility of the cations. In all cases, the conductivity of the pristine clay was much lower than for the composite material at temperatures below 600 K. For Li^+-exchanged clays, the conductivity at 550 K was 1 to 2 orders of magnitude greater than the Na^+-exchanged forms.[10]

Thin films of clay−polymer nanocomposites have a wide range of potential applications as barriers for gas transport and

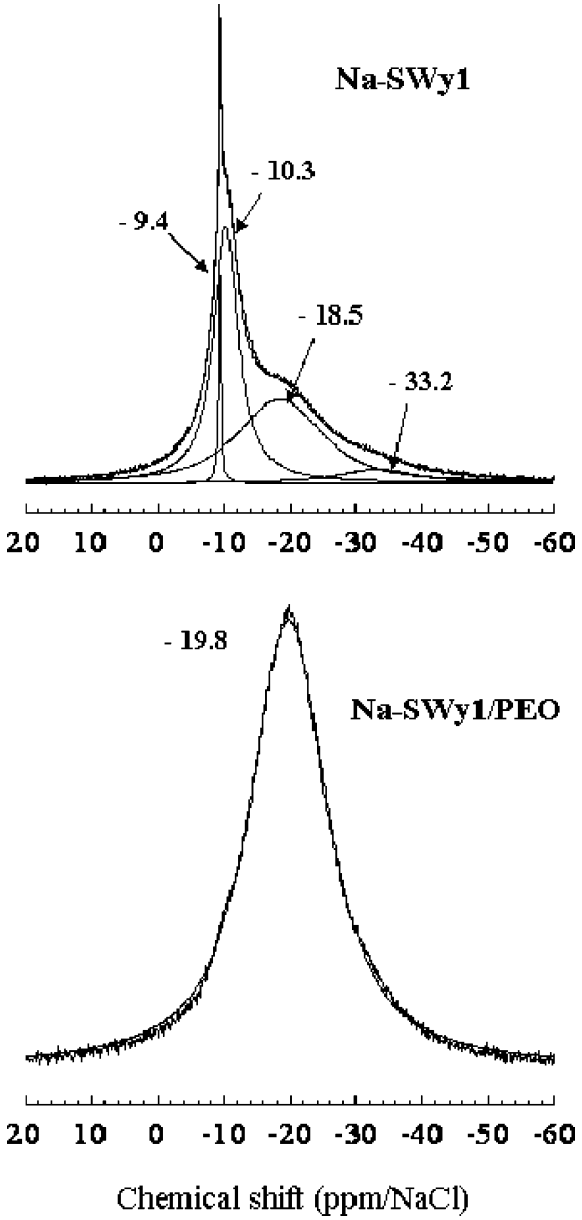

Figure 6. ^{23}Na MAS NMR spectra and their simulation for Na−SWy-1 in pristine (top) and PEO nanocomposite form at a 50:50 (w/w) clay: PEO ratio (bottom).

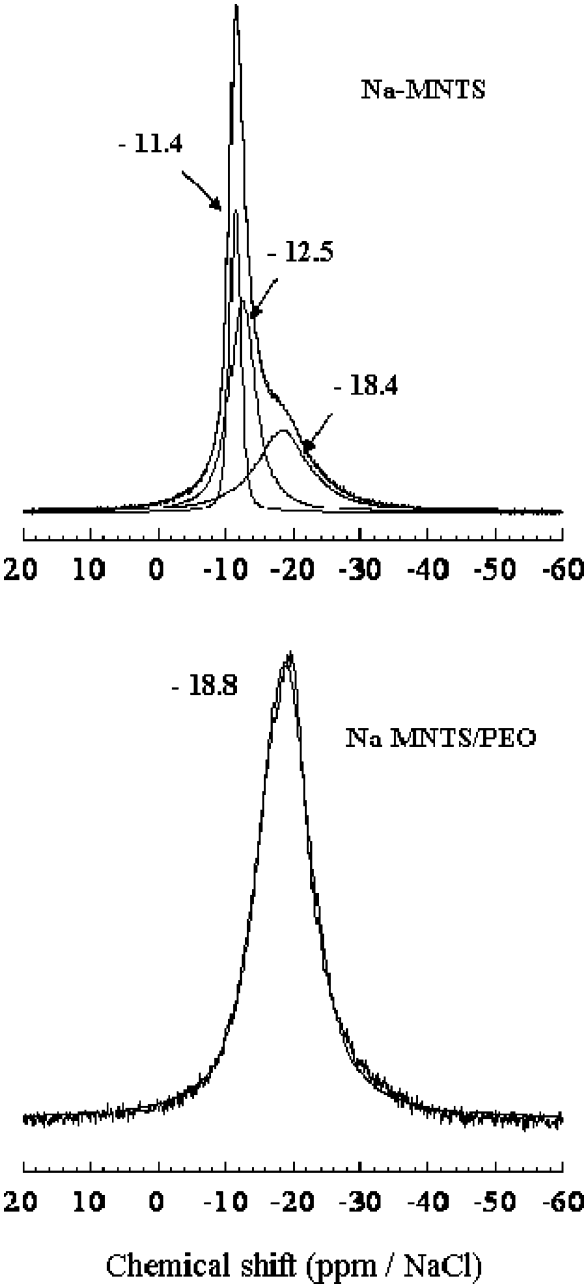

Figure 7. ^{23}Na MAS NMR spectra and their simulation for Na-MNTS in pristine (top) and PEO nanocomposite form at a 50:50 (w/w) clay: PEO ratio (bottom).

TABLE 3: ^{23}Na Resonances for Pristine Na^+ Montmorillonite and Selected PEO Composites

sample	chemical shift (ppm)	fwhm (Hz)
Na−SWy1	−9.4	60
	−10.3	600
	−18.5	2010
	−33.2	1790
Na−SWy1/PEO	−19.8	1840
Na−MNTS 100:0	−11.4	250
	−12.5	610
	−18.4	1220
Na−MNTS 50:50	−18.8	1200

as specifically oriented conducting materials. A thin film of Li^+−Laponite−PEO nanocomposite had a conductivity of 3.2×10^{-7} S cm^{-1} at 80 °C,[16] and Na^+−montmorillonite−polyethylene (PE) and −polyethylene-*block*-poly(ethylene glycol) (PE−PEG) thin film nanocomposites have a maximum conductivity of 2.5×10^{-5} S cm^{-1}.[17] Using puddle casting methods, Sandí et al. obtained composite films of a synthetic Li^+−hectorite and PEO with a conductivity of about 5.5×10^{-3} S cm^{-1} at 440 K,[18] the highest ever recorded for a clay nanocomposite. This exceptional conductivity may be due to either the larger size of synthetic hectorite particles compared to Laponite or to the presence of 20% amorphous silica in hectorite. In contrast to the work of Ruiz-Hitzky on the conformation of intercalated PEO, Wu and Lerner proposed the presence of one or two layers of polymer chains with nonhelical conformations in the galleries of Na−montmorillonite composites,[12] with the number of polymer layers increasing with increasing polymer/clay ratio. They proposed that the intercalation of PEO increases the mobility of cations by reducing their interactions with the negatively charged clay surface and that the observed decrease in conductivity with increasing temperature below the PEO decomposition temperature is due to a change in polymer conformation. Vaia and co-workers[13,14] and

Bujdák and co-workers[15] showed that layer charge can influence PEO intercalation for polystyrene−mica and PEO−smectite composites. Parallel molecular dynamics (MD) simulations demonstrated that PEO replaces the water molecules filling the space between the hydrated interlayer cations and that the polymer oxygen atoms do not interact directly with the cations. Instead, the cations are mostly coordinated to water and surface oxygen atoms.

In this work, the intercalation of PEO in the interlayers of natural (SWy-1) and synthetic (MNTS) montmorillonite is verified by the increased d_{001}-spacing for the nanocomposite samples in comparison to the pristine clays. The basal spacings of the pristine SWy-1 and MNTS samples correspond to a single water layer hydration state.[31,32] The (001) peak of pristine MNTS is broader than that of SWy-1, suggesting that restacking of the clay platelets during drying on the glass slide is more uniform for Swy-1. Intercalation occurs for Li^+-, Na^+-, and K^+-exchanged clay samples, and maximum basal spacings in the range 17.9−19.4 Å are achieved at overall clay:PEO ratios of 50:50 (w/w). For the SWy-1 composites, the maximum basal spacings are independent of the exchange cation, despite the K^+ form of the pristine clay being ∼0.4 Å more expanded. For the MNTS composites, the maximum basal spacing of the Li form is about 1.4 Å greater than that for the Na form at a 50:50 clay polymer ratio. These basal spacings suggest that the polymer is incorporated as a double layer of chains parallel to the silicate layer or as a single layer of PEO taking a helical conformation parallel to the layers.[9−12] Recent studies are pointing to a double-layer positioning of the polymer with no specific orientation of the chains in the mineral layer plane.[15,33,34] Nevertheless, the intercalation of PEO improves in all cases the stacking order of the layers, as indicated by the narrowing of the d_{001} diffraction peak.

The weight loss and exothermic features observed between 230 and 310 °C in the TGA-DTA curves for both the SWy-1 and the MNTS nanocomposites are unambiguously assigned to the combustion of the polymer. Thermal analysis also shows that the hydration state of the pristine SWy-1 clays increases in the order $K^+ < Na^+ < Li^+$, although the basal spacing for the Li^+ form is smaller than that for the Na^+ form. The K^+-exchanged SWy-1 clay is the least hydrated clay in both pristine and nanocomposite form. Finally, the TGA and DTA oxidation features for the MNTS−PEO composites appear at lower temperatures and occur over a more extended temperature range than those of the SWy1−PEO composites. The lower stability for the MNTS composites is most likely due to smaller mean particle diameters (smaller layer aspect ratios) relative to SWy-1. Smaller particle diameters facilitate transport of oxygen to the interlayer polymer. The poorer layer stacking order for the MNTS composites also is reflected in the broader d_{001} diffraction peaks.

These XRD and TGA/DTA results led us to favor PEO intercalation as double layer (XRD) and the partial replacement of the interlayer water upon PEO intercalation. This is in accord with small-angle X-ray scattering (SAXS) studies showing that PEO confined in clay interlayers has a noncrystalline structure[18] and with previous XRD, TGA, and Monte Carlo and molecular dynamics (MD) simulation studies.[15]

Variable temperature ^2H and ^7Li nuclear magnetic resonance (NMR) line widths and T_1 relaxation time studies of clay−polymer nanocomposites have shown that the characteristic time scale for cation diffusion is much shorter than that of segmental motion of the polymer.[24,25,35] In addition, simulations of asymmetric ^7Li NMR line shapes recorded at low temperature[26] and Monte Carlo and Molecular Dynamics computer simulations[33,34] show that Li^+ mobility is determined by the balance between the cation interaction with the PEO and the montmorillonite surface and the polymer segmental dynamics. Computed density profiles show the existence of three different interlayer Li^+ sites.[33] These are at the mid-interlayer, closer to the basal clay siloxane surface, and in the pseudohexagonal cavities of the tetrahedral sheet. ^7Li NMR line shape simulations also have demonstrated that Li^+ diffusivity in PEO intercalated compounds appears to be restricted by the inefficient linking of the Li^+ to the polymer chains and that most of the cation diffusion occurs as jumps along the basal oxygens of the silicate.[26] Additionally, the polymer chains are arranged in two distinguishable layers parallel to the silicate sheets,[26,33,34] and they retain a disordered, liquidlike structure with no preferred orientation of the backbone chain.[34]

Our ^7Li and ^{23}Na NMR spectra also provide important insights into the effects of PEO on the environment and dynamics of the interlayer cations. Although the ^7Li line shapes should be sensitive to local structural environmental changes,[24,25,35] the only effect observed upon increasing the degree of PEO, intercalation is a small amount of line broadening and a slightly more negative chemical shift. These observations suggest that Li^+ remains in the same structural environment regardless of the amount of intercalated PEO in the interlayer and that the ion interacts only weakly with PEO. In contrast, the ^{23}Na NMR results show the presence of Na^+ in multiple hydration states. These environments are distinguished by the inner-sphere or the outer-sphere coordination of clay oxygen atoms to the metal cation.[28,30] PEO intercalation causes the sodium to take on inner-sphere coordination. In such inner-sphere sites, the ion has a partial shell of water molecules and the remaining sites are probably occupied by oxygen atoms in the clay basal plane,[29,30] since SWy-1 has a permanent negative structural charge of 0.7 per formula unit, and nearly 40% of this is developed by tetrahedral Al for Si substitution. The reduction in interlayer water content with PEO intercalation in the SWy-1 samples depends on the interlayer cation, with the greatest effect for Li^+ and the least for Na^+. For the Li^+-exchanged samples, the reduction from 8.3 to 3.9 water molecules per formula unit does not affect the ^7Li NMR resonance significantly, indicating that the large hydration energy of Li^+ allows it to retain its hydration shell. In contrast, for Na^+ the reduction from 7.0 to 5.3 water molecules per formula unit results in a conversion of all the ions to inner-sphere sites resulting in an overall decrease in Na^+ hydration.

The differences in hydration behavior between Li^+ and Na^+ correlate well with the observation that the conductivity of Li−montmorillonite−PEO nanocomposites is up to 1 order of magnitude higher than the conductivity of Na−montmorillonite−PEO nanocomposites.[10] The formation of inner-sphere complexes by Na^+, as supported by our NMR results, retards its diffusional motion relative to Li^+, for which the local hydration environment does not change substantially in the presence of intercalated PEO. Indeed, the comparison of pristine Li^+- and Na^+-exchanged clays, and some other cation-exchanged clays, showed that their conductivity used to be of the same order of magnitude.[36,37] Reported conductivities for pristine Li^+ and Na^+ have ranged from 2×10^{-4} to 2×10^{-3} S cm^{-1}, depending on the clay,[36,37] to $(6-9) \times 10^{-9}$ S cm^{-1}.[38] These discrepancies for the pristine clays, together with those made on composite clays materials, demonstrate that the accurate determination of clay conductivity is quite difficult. Nevertheless, it is quite clear that Li^+ is much more conductive than

Na^+ in the presence of intercalated PEO and that the difference is correlated with the difference in hydration between the two cations. Thus, our results support the concept that PEO oxygen atoms do not sequester the exchangeable cations and that the site-hopping model advanced by Kuppa and Manias is responsible for ion transport.[34]

Acknowledgment. This research was supported in part by NSF Grant CHE-0211029 (T.J.P.) and by DOE Basic Energy Sciences Grant DEFGO2-00ER-15028 (R.J.K.).

References and Notes

(1) Dias, F. B.; Plomp, L.; Veldhuis, J. B. J. *J. Power Sources* **2000**, *88*, 169.
(2) Tarascon, J. M.; Armand, M. *Nature* **2001**, *414*, 359.
(3) Chen, H.-W.; Chiu, C.-Y.; Wu, H.-D.; Shen, I.-W.; Chang, F.-C. *Polymer* **2002**, *43*, 5011.
(4) Strawhecker, K. E.; Manias, E. *Chem. Mater.* **2003**, *15*, 844.
(5) Slane, S.; Salomon, M. *J. Power Sources* **1995**, *55* (1), 7.
(6) Mehrotra, V.; Giannelis E. P. *J. Appl. Phys.* **1992**, *72* (3), 1039.
(7) Liao, C.-S.; Ye, W.-B. *J. Polym. Res.* **2003**, *10*, 241.
(8) Chu, P. P.; Jaipal Reddy, M.; Kao, H. M. *Solid State Ionics* **2003**, *156*, 141.
(9) Ruiz-Hitzky, E.; Aranda, P. *Adv. Mater.* **1990**, *2* (11), 545.
(10) Aranda, P.; Ruiz-Hitzky, E. *Chem. Mater.* **1992**, *4*, 1395.
(11) Aranda, P.; Galvan, J. C.; Casal B.; Ruiz-Hitzky, E. *Electrochim. Acta* **1992**, *37* (9), 1573.
(12) Wu, J.; Lerner, M. M. *Chem. Mater.* **1993**, *5*, 835.
(13) Vaia, R. A.; Ishii, H.; Giannelis, E. P. *Chem. Mater.* **1993**, *5*, 1694.
(14) Vaia, R. A.; Vasudevan, S.; Krawiec, W.; Scanlon, L. G.; Giannelis, E. P. *Adv. Mater.* **1995**, *7* (12), 154.
(15) Bujdák, J.; Hackett, E.; Giannelis, E. P. *Chem. Mater.* **2000**, *12*, 2168.
(16) Doeff, M. M.; Reed, J. S. *Solid State Ionics* **1998**, *113*−*115*, 109.
(17) Liao, B.; Song, M.; Liang, H.; Pang, Y. *Polymer* **2001**, *42*, 10007.
(18) Sandí, G.; Joachim, H.; Kizilel, R.; Seifert, S.; Carrado, K. A. *Chem. Mater.* **2003**, *15*, 838.
(19) Leroux, F.; Aranda, P.; Besse, J.-P.; Ruiz-Hitzky, E. *Eur. J. Inorg. Chem.* **2003**, 1242.
(20) Reinholdt, M.; Miehé-Brendlé, J.; Delmotte, L.; Tuilier, M.-H.; Le Dred, R.; Cortès, R.; Flank, A.-M. *Eur. J. Inorg. Chem.* **2001**, *11*, 2831.
(21) Reinholdt, M.; Miehé-Brendlé, J.; Delmotte, L.; Le Dred, R.; Tuilier, M.-H. *Clay Miner.* **2005**, *40* (2), 177.
(22) Vantelon, D.; Pelletier, M.; Michot, L. J.; Barres, O.; Thomas, F. *Clay Miner.* **2001**, *36*, 369.
(23) Frost, R. L.; Ruan, H.; Kloprogge, J. T.; Gates, W. P. *Thermochim. Acta* **2000**, *346*, 63.
(24) Wong, S.; Vaia, R. A.; Giannelis, E. P.; Zax, D. B. *Solid State Ionics* **1996**, *86*−*88*, 547.
(25) Wong, S.; Zax, D. B. *Electrochim. Acta* **1997**, *42* (23−24), 3513.
(26) Yang, D. K.; Zax, D. B. *J. Chem. Phys.* **1999**, *110* (11), 5325.
(27) Arun, N.; Vasudevan, S.; Ramanathan, K. V. *J. Chem. Phys.* **2003**, *119* (5), 2840.
(28) Liang, J.-J.; Sherrif, B. L. *Geochim. Cosmochim. Acta* **1993**, *57*, 3885.
(29) Xue, X.; Stebbins, J. F. *Phys. Chem. Miner.* **1993**, *20*, 297.
(30) Kim, Y.; Kirkpatrick, R. J. *Geochim. Cosmochim. Acta* **1997**, *61* (24), 5199.
(31) Watanabe, T.; Sato, T. *Clay Sci.* **1988**, *7*, 129.
(32) Yamada, H.; Nakazawa, H.; Hashizume, H.; Shimomura, S.; Watanabe, T. *Clay Miner.* **1994**, *42* (1), 77.
(33) Hackett, E.; Manias, E.; Giannelis, E. P. *Chem. Mater.* **2000**, *12*, 2161.
(34) Kuppa, V.; Manias, E. *Chem. Mater.* **2002**, *14*, 2171.
(35) Wong, S.; Vasudevan, S.; Vaia, R. A.; Giannelis, E. P.; Zax, D. B. *J. Am. Chem. Soc.* **1995**, *117*, 7568.
(36) Liu, J.; Pan, J.; Chen J. *Solid State Ionics* **1995**, *82*, 225.
(37) Fan, Y.; Wu, H. *Solid State Ionics* **1997**, *93*, 347.
(38) Mandair, A.-P.; McWhinnie, W. R.; Monsef-Mirzai P. *Inorg. Chim. Acta* **1987**, *134*, 99.